Journal of Materials Chemistry A

Accepted Manuscript

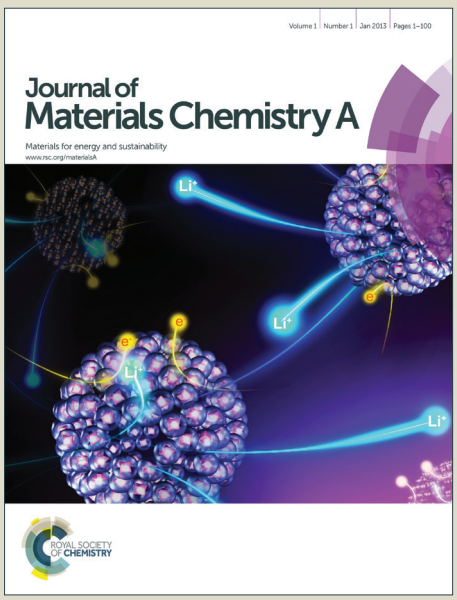

ROYAL SOCIETY OF CHEMISTRY

www.rsc.org/materialsA

Journal of
Materials Chemistry A

RSCPublishing

ARTICLE

High-index-faceted platinum nanoparticles: Insights into structural, thermal stabilities, and shape evolution from atomistic simulations

Cite this: DOI: 10.1039/xoxxooooox

Received ooth January 2014,
Accepted ooth January 2014

DOI: 10.1039/xoxxooooox

www.rsc.org/

Xiang-Ming Zeng,[a] Rao Huang,[a] Gui-Fang Shao,[b] Yu-Hua Wen,[*,a] and Shi-Gang Sun [c]

High-index-faceted Pt nanoparticles exhibit exceptional electrocatalytic activity owing to high density of low coordination sites on surface, thus have attracted extensive studies over the past few years. In this article, we employed atomistic simulations to systematically investigate the structural, thermal stabilities and shape evolution of Pt nanoparticles with different high-index facets, that is, tetrahexahedra enclosed by {*hk*0} facets, trapezohedra by {*hkk*} ones, and trisoctahedra by {*hhk*} ones. The results show that {221} faceted trisoctahedral nanoparticles display the best structural and thermal stabilities while {410} faceted tetrahexahedral ones do the worst. The shape stability of these nanoparticles generally decreases in the order from trapezohedron and tetrahexahedron to trisoctahedron. For the same type of polyhedron, the structural, thermal and shape stabilities of the nanoparticles all decreases according to the order of {2*kl*}, {3*kl*} and {4*kl*} facets. Further analyses have discovered that a large proportion of high-coordinated surface atoms are beneficial to enhancing both the thermal and the shape stabilities. This work provides an in-depth understanding of surface structures and thermodynamic evolutions of high-index-faceted metallic nanoparticles.

1. Introduction

Platinum nanoparticles (NPs) are widely used as indispensible catalysts in fuel cells, petrochemical reforming and automotive catalytic converters due to their excellent activity and stability[1-3]. The rare reserve and high cost of Pt, however, severely limit its further usage. In order to meet the increasing demand in industry, how to improve the intrinsic catalytic properties and utilization efficiency of Pt NPs therefore becomes a key issue in the development of industrial catalytic fields.

As is well-known, the exceptional chemical (especially the catalytic) and physical properties of NPs are strongly dependent not only on the particle sizes but also on their surface structures, that is, the crystallographic surfaces that enclose the particles[4-8]. Since the crystallographic surface directly determines the particle shape, the shape-controlled synthesis of NP catalysts hence becomes a promising route for precisely tuning their catalytic activity and selectivity. After the pioneering work of El-Sayed *et al.* for the synthesis of cubic and tetrahedral Pt NPs[9], considerable efforts have been devoted to preparing Pt NPs with different shapes by changing Pt precursors, reducing reagents, stabilizing reagents, and solvents. In the past decades, various Pt NPs with well-defined shapes have been experimentally synthesized while most of them were enclosed by low-index planes[6,7,10-14]. For examples, the cube is bound by {100} facets, tetrahedron, octahedron, decahedron, and icosahedron by {111} facets, cuboctahedron and truncated octahedron by {100} and {111} facets. Nevertheless, fundamental studies on metal single-crystal surfaces have demonstrated that Pt high-index planes with open surface structures exhibit much higher reactivity than {111} or {100} low-index ones because they have a large density of low-coordinated atoms situated on steps, ledges and kinks with high reactivity required for high catalytic activity[15,16]. More importantly, on high-index planes, there exist short-ranged steric sites (such as "chair" sites) that consist of several (typical 5-6) step and terrace atoms and are considered as active sites[3,17]. Because of the synergistic effect between the step and terrace atoms, these steric sites usually

serve as catalytically active sites and also display high stability[3,17]. Naturally, high-index planes are expected to be introduced into Pt NPs for enhancing their catalytic activity and stability. However, during the crystal growth process, the high-index planes that have high surface energy would be completely eliminated since thermodynamics of crystallization usually requires the minimization of the total surface energy of the crystal. It is, therefore, a great challenge to synthesize Pt NPs with high-index facets due to their high surface energy. Fortunately, an important breakthrough was achieved in 2007 by Sun *et.al*., who successfully obtained tetrahexahedral Pt NPs bound with {730} and vicinal high-index facets by developing an electrochemical square-wave potential method[18]. As was expected, these unusual Pt NPs exhibited both good stability and greatly enhanced catalytic activity compared with the existing commercial Pt catalysts[18-19]. Subsequently, tetrahexahedral Au, Pd, Au-Pd, and Pd-Pt NPs have been prepared by the electrochemical and wet-chemical methods[20-24]. Furthermore, trapezohedral Pt with {522} facets[25,26], trisoctahedral Au with {221} facets[27,28] and Au-Pd NPs with {331} facets[29] have also been reported in the following years. Recently, Sun *et.al* successfully synthesized complex convex hexoctahedral Pt NPs enclosed by 48 {1553} high-index facets by the electrochemical route[30]. These NPs are even more complicated than the tetrahexahedral, trapezohedral and trisoctahedral ones, their shape is the last single crystal form that had not been achieved previously for face-centered-cubic (fcc) metals. The aforementioned studies have stimulated great interest in synthesis, characterization and structure-property relationship of Pt NPs with high-index facets.

Despite the fact that the synthesis and catalytic properties of high-index-faceted Pt NPs have been extensively investigated[18-30], to the best of our knowledge, less is known about their structural and thermodynamic stabilities. Although the surface energies of different crystalline planes were well known for fcc bulk metals[31], it is unascertained whether the order of these surface energies remains valid for fcc metal NPs with the particle sizes decreasing to several tens of nanometers or even less because of the pronounced proportion of terrace, step and kink atoms at surface. Meanwhile, the thermodynamic stability of NPs is of considerable importance for their chemical synthesis and ultimate applications owing to the following two reasons: On one hand, the NPs tend to aggregate into larger particles due to the enhanced atomic diffusion when the ambient temperature reaches the Tammann temperature[32]. Thus, to reasonably control the synthesis and catalytic temperature is of technological importance for preventing their sintering and coarsening. On the other hand, catalytic reactions generally occur on surface of NPs[2], their surface structures will hence play a critical role in the catalytic processes. However, the catalytic reactions usually take place at high temperature situations such as in cracking of petroleum and purification of automobile exhaust gases where the particle shapes cannot be retained. Once the high-index-faceted surface is destroyed, the NPs will lose their excellent catalytic properties. Therefore, understanding the structural and thermodynamic stabilities of Pt NPs is considerably helpful not only for suppressing their sintering and coarsening but also for stabilizing their high-index-faceted surface structures at elevated temperatures.

In this article, we have addressed on studies of structures and stabilities of Pt NPs with high-index facets by means of atomistic simulations. There have been investigated three types of polyhedral Pt NPs, *i.e.*, tetrahexahedral, trapezohedral, and trisoctahedral ones. To our knowledge, this is the first systematic report about the thermodynamic stability and shape evolution of high-index-faceted fcc metal NPs. This article is structured as follows. A brief description of the simulation methods is given in the following section. Section 3 presents the calculated results, discussion and comparison with available results. The main conclusions are summarized in the fourth section.

2. Simulation Methodology

As we know, different crystallographic planes determine various shapes of NPs[3,17]. For fcc metals such as Pt, Pd, Au and Ag, a unit stereographic triangle is often used to illustrate the polyhedral NPs enclosed by different crystal planes, as shown in Fig. 1. The polyhedral NPs located at the three vertexes are bound by low-index facets, *i.e.*, cube by {100}, octahedron by {111}, and rhombic dodecahedron by {110}. The polyhedral ones, lying in the sidelines of the triangle, are covered by high-index facets, *i.e.*, tetrahexahedron (THH) by {*hk0*}, trapezohedron (TPH) by {*hkk*}, and trisoctahedron (TOH) by {*hhk*} with at least one Miller index being larger than unit. These three kinds of polyhedra have twenty-four facets and open surface structures. The polyhedra inside the triangle are hexoctahedron (HOH) enclosed by forty-eight {*hkl*} ($h>k>l>0$) facets[30]. It should be noted that high-index planes can be composed of basal high-index ones. For example, the {730} surface is periodically composed of two {210} subfacets followed by one {310} subfacet, the {1030} surface is periodically composed of two {310} subfacets followed by one {410} subfacet, and the {522} surface is periodically composed of one {211} subfacet followed by one {311} subfacet. Therefore, {*h*10}, {*h*11} and {*hh*1} (*h*=2-4) surfaces may be regarded as representatives of high-index planes. In this article, we will address three types of polyhedral Pt NPs, that is, THH, TPH, and TOH ones enclosed by respective basal high-index facets. In order to reasonably correspond to the structure and shape of NPs observed experimentally, they were initially constructed from a large cubic fcc single crystal. Similarly, a series of Pt NPs with different sizes and shapes were modeled. Due to the limitation of present computer facilities available, the total number of atoms in Pt NPs varies between 200 and 550,000.

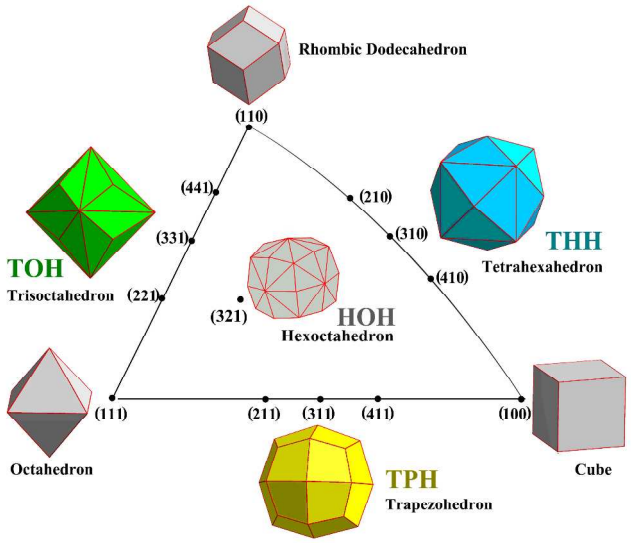

Fig. 1 Unit stereographic triangle of polyhedral Pt NPs enclosed by different crystal planes.

In atomistic simulations, the quantum corrected Sutton-Chen (Q-SC) type many-body potentials [33] were applied to describe the interatomic interactions. These potentials belong to the scheme of embedded-atom method (EAM),[34,35] and represent many-body interactions. Their parameters are optimized to describe the lattice parameter, cohesive energy, bulk modulus, elastic constants, phonon dispersion, vacancy formation energy, and surface energy, leading to an accurate description of many properties of fcc metals and their alloys.[36-42] According to the framework of Q-SC potentials, the total potential energy for a system of atoms can be written as

$$U = \sum_i U_i = \sum_i \varepsilon \left[\frac{1}{2} \sum_{j \neq i} V(R_{ij}) - c\sqrt{\rho_i} \right], \qquad (1)$$

in which $V(R_{ij})$ is a pair interaction function defined by the following equation:

$$V(R_{ij}) = \left(\frac{a}{R_{ij}} \right)^n, \qquad (2)$$

accounting for the repulsion between the i and j atomic cores; ρ_i is a local electron density accounting for cohesion associated with atom i defined by

$$\rho_i = \sum_{j \neq i} \left(\frac{a}{R_{ij}} \right)^m. \qquad (3)$$

In Eqn. (1)–(3), R_{ij} is the distance between atoms i and j; a is a length parameter scaling all spacings (leading to dimensionless V and ρ); c is a dimensionless parameter scaling the attractive terms; ε sets the overall energy scale; n and m are integer parameters such that $n>m$. Given the exponents (n,m), c is determined by the equilibrium lattice parameter, and ε is determined by the total cohesive energy. The model parameters for Pt are given as follows: n=11, m=7, ε=9.7894 *meV*, c=71.336, and a=3.9163 Å.[33]

As the first stage of atomistic simulations, the energy minimization scheme should be applied to search the lowest-energy configurations of the modeled NPs. Note that the total energy at absolute zero can be obtained by summing the potential energy of each atom in the NPs. However, the prediction of energetically most stable structures is highly complicated for such NPs because it requires searching the minimum points on the potential energy surface, which corresponds to the stable states of the systems. Therefore, the conjugate gradient methods (CGM) were used for the energy minimization of Pt NPs with fixed shapes.[43]

After initial energy minimization, molecular dynamics (MD) methods were employed to simulate the continuous heating process. In order to facilitate a comparison of different polyhedra, the total atomic number of all the heated NPs was selected to be about 20, 000, corresponding to a particle size of about 8.3 nm. To make the simulations more reliable, we employed constant temperature and pressure molecular dynamics (NPT-MD) to allow energy and volume fluctuations, which may be critical to the resulting dynamics. The NPs underwent the heating process consisting of a series of NPT-MD simulations from 0 to 2200 K with a temperature increment of 50 K. However, a smaller step of 10 K was adopted to investigate the melting behavior more accurately when the temperature reached to around the melting point. The simulations were carried out for 200 ps of the relaxation time at each temperature, and the statistical quantities were obtained in the last 25 ps. The desired temperature and ambient pressure were maintained by Nose-Hoover thermostat [44] and Berendsen "pressure bath" [45], respectively. The equations of atomic motion were integrated by the Verlet-Velocity algorithm [46] with a time step of 1.0 fs.

3. Results and Discussion

3.1 Structural stability

It is well known that the particle of lower energy tends to be energetically more stable. To facilitate comparison of structural stability of Pt NPs with different shapes and surface structures, a common definition of particle size based on equivalent volume was introduced here

$$d = \sqrt[3]{\frac{3N}{2\pi}} a_0, \qquad (4)$$

where N is the total number of atoms in the NPs, and a_0=3.924 Å is the lattice constant of bulk Pt. Since there are four atoms in each unit cell for fcc crystals, the equivalent volume of each atom can be considered as $a_0^3/4$. Fig. 2a and 2b show the size-dependent energy at ground state for the relaxed Pt NPs of size up to 30 nm. In order to further investigate the structural stability of Pt NPs with larger sizes, we express the total energy according to the NP constitution. Considering that a polyhedral NP consists of atoms located in its interior, facets, edges, and vertices, the average energy per atom of the NP can be expressed by the formula as follows

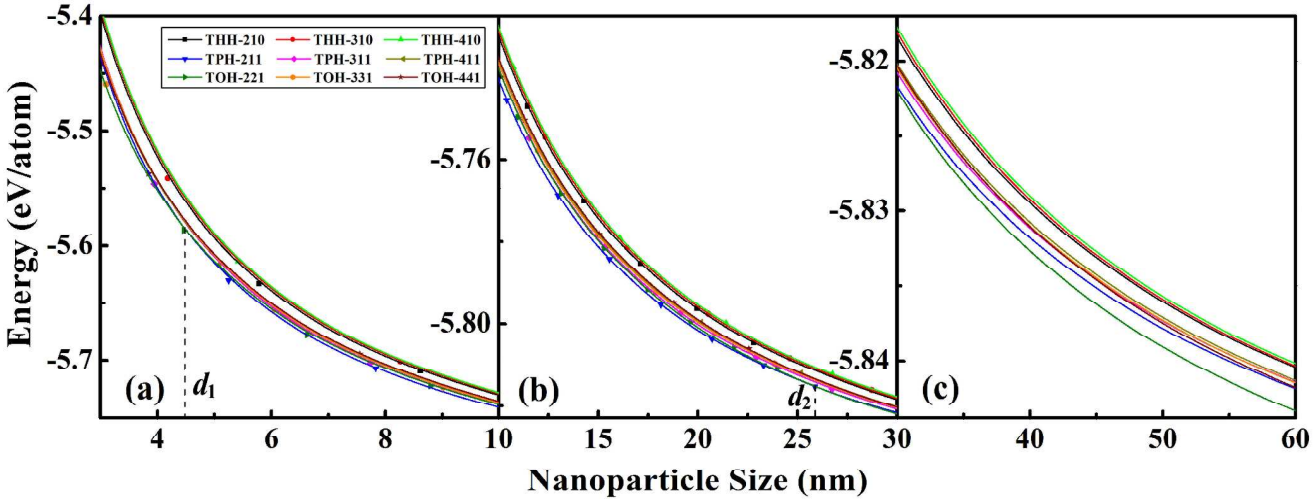

Fig. 2 Size-dependent energies of Pt NPs with different high-index facets. The results presented in (c) from the fitting curves for Pt NPs with size from 3 to 30 nm. Note that d_1=4.5 nm and d_2=25.9 nm denote the cross point between {211} and {221} facets.

$$\overline{E} = \frac{1}{N}(N_i\overline{E}_i + N_f\overline{E}_f + N_e\overline{E}_e + N_v\overline{E}_v) = A_1 + \frac{B_1}{d} + \frac{C_1}{d^2} + \frac{D_1}{d^3}, \quad (5)$$

where N, N_i, N_f, N_e, and N_v is the atomic number of the system, interior, facets, edges, and vertices, respectively, $\overline{E}$, $\overline{E}_i$, $\overline{E}_f$, $\overline{E}_e$, and $\overline{E}_v$ is the average energy per atom of the system, interior, facets, edges, and vertices, respectively. This polynomial function was accordingly used to fit the data of energy within the framework of the least square method. Fig. 2a and 2b show that the fitted curves are in good agreement with the calculated data. In order to further examine the structural stability of larger particle, the curves were extrapolated to 60 nm, as illustrated in Fig. 2c.

As seen from Fig. 2, strong size effects are found from the pronounced decrease in potential energy as the particle size increases. Although there is no significant prominence in structural stability among different shaped Pt NPs, the distinguishable energy differences still indicate that surface structure plays a key role in determining the stability of Pt NPs. Generally, TPH and TOH NPs exhibit similar stabilities, and both of them have better stability than THH ones. In spite of the small energy difference, the {211} faceted TPH is ascertained to be the most stable shape when the particle size is larger than 4.5 nm. However, the first place is substituted by the {221} faceted TOH NP when the particle size exceeds 25.9 nm, as indicated by Fig. 2b. As for the THHs, the structural stability of three faceted NPs decreases in the order of {210}, {310}, {410}, and they all exhibit wore stability than the other NPs under the particle size of 60 nm, as shown in Fig. 2c. Further analyses show that the order of {211}>{311}>{411} and {221}>{331}>{441} is also valid for the structural stability of TPHs and TOHs, respectively (see Fig. 2). Since there is no distinct energy difference in interior atoms, the discrepancies of the average atomic energy among different polyhedral Pt NPs are contributed by surface atoms. These discrepancies will be less remarkable with the growing particle size due to the decreasing surface-to-volume ratio.

In order to highlight the contribution of atomic sites on surface, similar to the average energy per atom, the surface energy of NP were calculated and fitted according to the formula as follows

$$\gamma = \frac{\sum_{i=1}^{N} E_i - NE_{bulk}}{S} = A_2 + \frac{B_2}{d} + \frac{C_2}{d^2} + \frac{D_2}{d^3}, \quad (6)$$

where S is the total surface area of the NP. Both the calculated surface energies and fitted curves are illustrated in Fig. 3.

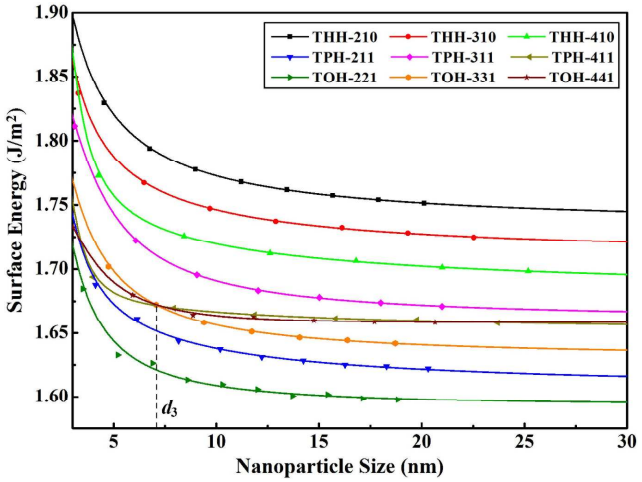

Fig. 3 Surface energy as a function of NP size. Note that d_3=7.1 nm denotes the cross point between {331} and {441} facets.

The fitted curves display an excellent accordance with the calculated values. It can also be observed from this figure that the surface energies of different high-index-faceted NPs are generally increased in the order of $\gamma_{\{221\}} < \gamma_{\{211\}} < \gamma_{\{331\}} < \gamma_{\{441\}} < \gamma_{\{411\}} < \gamma_{\{311\}} < \gamma_{\{410\}} < \gamma_{\{310\}} < \gamma_{\{210\}}$ when the particle size is beyond 7.1 nm or so. For convenience of comparison, we also calculated the surface energies of the corresponding high-index planes in semi-infinite crystals. The results show that the surface energy is 1.744, 1.725, 1.706, 1.62, 1.669, 1.665, 1.594, 1.633, and 1.651 J/m^2 for the {210}, {310}, {410}, {211}, {311}, {411}, {221}, {331}, and {441} surfaces, respectively. One can find from Fig. 3 that the order of surface energy for large NPs (typical larger than 10 nm) is well consistent with the result in infinite surfaces. Generally speaking, it

is acceptable that the lower surface energy leads to better structural stability, which may be used to explain why the {221} faceted TOH is the most stable in high-index-faceted NPs. Contrarily, the {210} faceted THH should possess the worst stability because the surface energy of {210} plane is the highest among all the considered surfaces. However, the least stable configuration does not occur in the THH enclosed by {210} facets but by {410} ones, as indicated by Fig. 2. Similarly, the surface energy of {331} plane is lower than that of {441} one, while the stability of the {331} faceted TOH is worse than the {441} faceted one for large NPs. These results signify that the surface energy is a crucial, but not the sole, factor in determining the structural stabilities of NPs. The final stabilities of the NPs are also associated with other factors such as the ratio of surface atoms to total number of atoms.

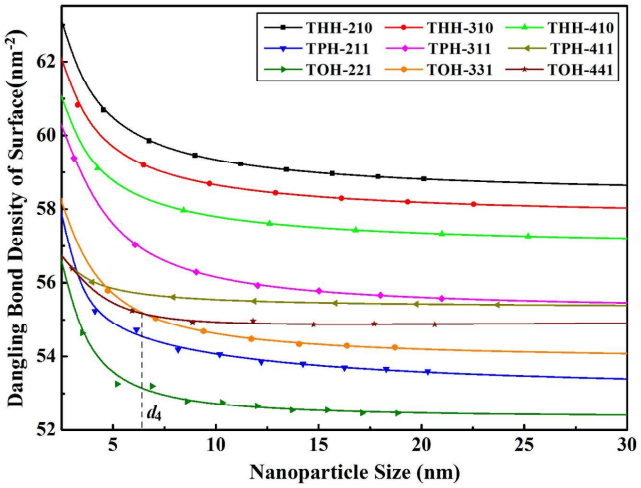

Fig. 4 Dangling bond density of surface as a function of NP size. Note that d4=6.4 nm denotes the cross point between {331} and {441} facets.

As is known, the catalytic reactions usually occur at surfaces. Therefore, investigation on the atomic bonding characteristics of surface is of great importance to understanding the catalytic activities and efficiencies of Pt NPs. The atomic bonding states of surface are generally featured by the concept of "dangling bond" number which denotes the lost of atomic coordination number (CN). The CN is equal to twelve for fcc metal atoms. Comparing with the bulk, the breaking of symmetry on NP surface leads to lower CNs of surface atoms. Here, the dangling bond density is defined as the number of dangling bonds per unit surface area. Generally, the high dangling bond density is beneficial to enhancing the surface catalytic activities. Considering the surface constitution of NP, we expressed the dangling bond density based on the formula as follows

$$\sigma = \frac{N_f \overline{D}_f + N_e \overline{D}_e + N_v \overline{D}_v}{S} = A_3 + \frac{B_3}{d} + \frac{C_3}{d^2}, \quad (7)$$

where $\overline{D}_f, \overline{D}_e, \overline{D}_v$ is the average dangling bond number of atoms on facets, edges, and vertices, respectively. We applied the above equation to fit the calculated data using least square method, and the fitted curves were presented in Fig. 4.

Evidently, the dangling bond density increases with the decreasing particle size, showing a strong size effect. Moreover, analogous to the surface energy, the dangling bond densities of the nine surfaces increase in the order of {221}, {211}, {331}, {441}, {411}, {311}, {410}, {310} and {210} when the particle size is larger than 6.5 nm. The results showed that the dangling bond densities of three types of polyhedra roughly follow the order of TOH<TPH<THH, indicating that the THH NPs would possess better catalytic property than the other two ones. By contrast, the {221} faceted TOH has the lowest dangling bond density although it exhibits the best structural stability. Therefore, a compromise should be acheived between the structural stability and the catalytic reactivity in the design or application of high-performance nanocatalysts. Interestingly, recent experiments have verified that the TPH NPs, which possess medium structural stability and dangling bond density can be evolved from THH through the electrochemical square-wave-potential method[30]. This shows that the surface structures and catalytic properties of high-index-faceted NPs may be continuously tuned by the electrochemical route, indicating that the compromise would be experimentally feasible.

3.2 Thermal stability

Owing to the potential applications of Pt NPs in high temperature environment, a natural motivation has arisen to examine the temperature dependence of stabilities under heating process. Important information involving the thermodynamic properties, the feature and development of melting can be obtained from the output data in MD simulations. As is known, the caloric curves (energy versus temperature) have been successfully applied to investigate the solid-liquid phase transition of NPs, nanowires, and bulk materials both theoretically and experimentally[37-42,47,48]. The solid-liquid phase transition temperature (T_m) is usually defined as the temperature at which the heat capacity reaches its maximum. We calculated the average potential energy during the heating process and then deduced the heat capacity according to following equation[37]

$$C_p(T) = \frac{dU}{dT} + \frac{3}{2} R_{gc}, \quad (8)$$

where U is the potential energy, and R_{gc}=8.314 J/molK.

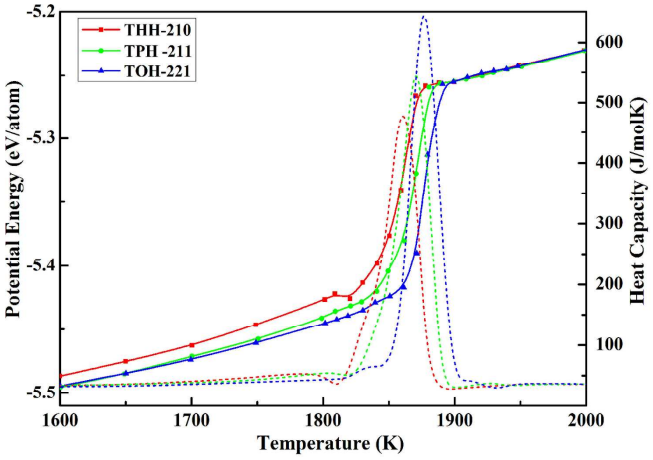

Fig. 5 Temperature dependence of potential energies and specific heat capacities of Pt NPs with different shapes. Note that the dashed lines correspond to the heat capacity.

Fig. 5 shows the temperature dependence of potential energy and heat capacity for three types of polyhedral Pt NPs. It can be seen from Fig. 5 that the potential energy exhibits a linear increase with

the rising temperature until 1700 K, corresponding to a steady heat capacity. When the temperature was further increased, a sharp rise of the potential energy and a keen-edged peak of the heat capacity occurred at the temperature of about 1870 K. The melting temperatures of all Pt NPs are notably lower than that of Pt bulk (2045 K for experimental value and 2090 K for theoretical calculation)[49,50]. Generally, this reduction should be attributed to high surface-volume-ratios in nano-sized particles and low surface premelting temperatures associated with the weak bonds in low-coordinated surface atoms, which has been demonstrated by numerous experimental and theoretical studies[47,48,51]. Due to the approximately equal size of the nine Pt NPs, the discrepancy of melting points is not pronounced but still distinguishable. For example, the melting temperature of the {221} faceted TOH NP is 20 K higher than that of the {210} faceted THH one (see Fig. 5). This result may be mainly attributed to the lower surface energy and higher average CN of surface atoms in the former than those in the latter, which leads to a higher premelting temperature and thus a higher melting point. Similarly, it can be used to elucidate why the melting point of the {211} faceted TPH NP is 10 K higher than that of the {210} faceted THH one (see Fig. 5). Analogous phenomena occurring in alloy NPs have also validated the dependence of melting behavior on surface properties such as CNs of surface atoms and surface energy[52].

In order to obtain an in-depth understanding of the melting mechanism of Pt NPs, it is necessary to investigate the detailed melting processes of these NPs during continuous heating. Generally, the melting mechanism can be explored by analyzing the structural evolution, diffusion coefficients, root-mean-square displacement of atoms and so on. Currently, the Lindemann index is a simple but effective measurement in characterizing the thermal evolution of a system[53]. For a system of N atoms, the local Lindemann index for the ith atom is defined as the root-mean-squared bond length fluctuation[54]

$$\delta_i = \frac{1}{N-1}\sum_{j\neq i}\frac{\sqrt{\langle R_{ij}^2\rangle - \langle R_{ij}\rangle^2}}{\langle R_{ij}\rangle}, \quad (9)$$

and the system-averaged Lindemann index is calculated as

$$\delta = \frac{1}{N}\sum_i \delta_i, \quad (10)$$

where R_{ij} is the distance between the ith and jth atoms. The Lindemann index was originally developed to study the melting behavior of bulk crystals. The Lindemann criterion suggests that the melting occurs when the index is in the range of 0.1-0.15, depending on materials. However, a smaller critical index of about 0.03 was commonly applied in clusters and homopolymers owing to the relaxed constraint of the surface atoms[55].

The temperature dependence of Lindemann indices during the heating process were calculated for all types of Pt NPs. In order to visually describe the melting process, we extracted the coordinates of all atoms in the Pt NPs at different temperatures. As a representative, Fig. 6 presents the atomistic snapshots of TPH covered by {211} facets, TOH by {221}, and THH by {210} at four temperatures. Here, the concept of Lindemann atoms was introduced: The atom whose Lindemann index exceeds the critical value is defined as Lindeamnn atom; otherwise, it is marked as non-Lindemann atom. We find that 0.039 is the appropriate critical value of Lindemann index by investigating the Lindemann index curves during the continuous heating.

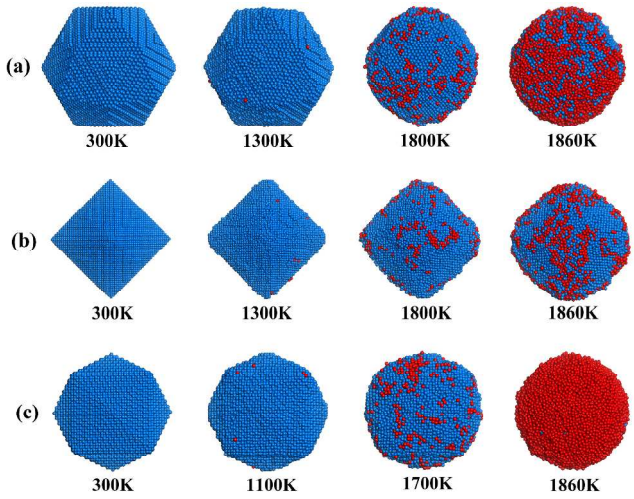

Fig. 6 Snapshots of Pt NPs with different shapes taken at four representative temperatures.(a) trapezohedron enclosed by {211} facets, (b) trisoctahedron by {221} ones, (c) tetrahexahedron by {210} ones. Coloring denotes type of atom: dodger blue, non-Lindemann atom; red, Lindemann atom.

As shown in Fig. 6, each Pt NP can retain its initial shape and surface structure at room temperature of 300 K. However, evident differences emerged in the subsequent structural evolutions of different types of NPs. It is found that the {211} faceted TPH can basically keep its original shape and surface structure up to 800 K or so (not presented here). With the temperature further increasing, the corner atoms near kinks firstly began to diffuse, while the atoms at six apexes remained at their initial positions. As the temperature went up to 1300 K, the apex atoms have already migrated from their initial positions and diffused inward (see the second picture in Fig. 6a). Nevertheless, the shape of TPH preserved well since the {211} facets were still be differentiable. Further heating accelerated the movement of surface atoms, resulting in the destruction of its surface structure and well-defined shape. At 1800 K, one can see that the TPH NP has transformed into a sphere-like one, and a number of Lindemann atoms appeared on the surface at this time, indicating the initiation of surface premelting. However, the majority of surface atoms belonged to non-Lindemann atoms were still resident on the original {111} subfacets. When the temperature increased to 1860 K, most of surface atoms have changed into Lindemann atoms, and surface atomic arrangements have been completely disordered, suggesting that the premelting has extended over almost the whole surface of the TPH Pt NP.

Comparing with the TPH NP, the TOH one covered by {221} facets exhibited similar melting behavior. Its original shape and structure can also be kept as the temperature went up to 800 K. With the temperature further increasing, the apex and corner atoms preferentially diffused away. Consequently, the apexes and edges became blunt and gradually disappeared at 1300 K, as depicted in Fig. 6b. At 1800 K, the occurrence of the Lindemann atoms indicated the beginning of surface premelting. Whereas, before transforming into a sphere, the TOH NP maintained a truncated-

octahedron-like shape for quite a long period. At 1860 K, the majority of surface atoms have not changed into Lindemann atoms, indicating that the {221} faceted TOH has a better thermal stability than the {211} faceted TPH. This is in good agreement with the result of their melting temperatures in Fig. 5. Besides, it is worth noting that the {211} facets on TPH surface can be composed of three atomic width (111) terraces separated by one step with monatomic height in the (100) direction, and the {221} facets on TOH surface can consist of three atomic width (111) terraces followed by single step with monatomic height in the (110) direction. Therefore, it is comprehensible to observe similar melting mechanism in these NPs.

As for the THH terminated by {210} facets, a worse thermal stability can be found from Fig. 6c. Those atoms at eight corners firstly diffused away. Subsequently, the atoms at six apices gradually disappeared at 1100 K. The coordination number analysis shows that the former are three-coordinated, and the latter are four-coordinated, implying that the less-coordinated atoms diffuse away more easily at the elevated temperature. With the temperature further rising, some atoms on the edges also started to move from their original positions. At 1300 K, all corners have completely disappeared, and the edges have become obtuse although the atomic steps were still resident on the surface (not presented here). However, the noticeable surface premelting occurred at 1700 K, which is lower than 1800 K of the abovementioned two particles. At 1860 K, all the surface atoms have evolved into Lindemann atoms, implying the premelting has extended over the entire surface and spread into the interior region progressively. At this time, the NP can be regarded as a mixture consisting of a liquid shell and a solid core. This mixture is chemically interesting because the liquid metal atoms on the surface of solid particles could facilitate the dissolution of adsorbates due to their enhanced mobility, enabling the occurrence of different chemical processes[56]. Evidently, the complete melting of surface for the THH NP is prior to the TPH and TOH NPs. Considering that the {210} facets on THH are periodically composed of two (100) terraces followed by one (110) steps which are both less stable than the {111} subfacet, it is not surprising to observe the worst thermodynamic stability of the {210} faceted THH NP among these three particles. Further increased temperature resulted in the overall melting of THH NP and the formation of a typical liquid NP.

Furthermore, analogous to the above analyses, it can be found that, for the same type of polyhedron, the thermal stability of Pt NPs decreases according to the order of {2kl}, {3kl} and {4kl} facets, which is similar to the order of structural stability.

3.3 Shape stability

It is well-known that surface structure characteristics of NPs determine their catalytic properties because the catalytic reactions preferentially take place on surface. From the aforementioned discussion, we can see that Pt NPs of different shapes lost their orderly surface structures at elevated temperatures, and finally evolved into sphere-like ones prior to the overall melting. Owing to the fact that the destruction of surface structure would lower their catalytic activities, it is crucial to identify the critical temperature of surface structure transformation for both the design and application of NP catalysts. Note that the shapes of polyhedra are strongly dependent on the surface structure, thus the shape change is indicative of surface structure transformation. To accurately describe the shape evolution, here we introduce the shape factor S as follows[57]

$$S = \frac{1}{R^2}\sqrt{\frac{1}{\mathrm{N}}\sum_{i=1}^{N}(r_i^2 - R^2)^2}\ , \qquad (11)$$

in which r_i is the distance of atom i from the particle center of mass and R is the root-mean-square of r_i,

$$R = \sqrt{\frac{1}{\mathrm{N}}\sum_{i=1}^{N} r_i^2}\ . \qquad (12)$$

According to the definition above, the shape factor is a sensitive indicator of particle shape, independent of total atomic number in the particle. Fig. 7 illustrates the temperature dependent shape factors for the nine Pt NPs.

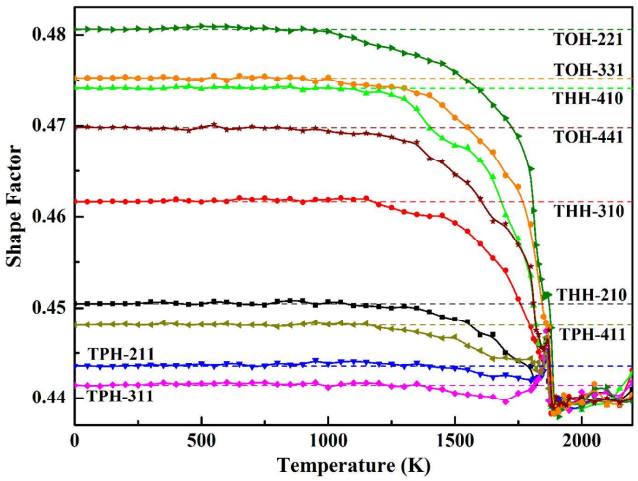

Fig. 7 Shape factors of different high-index-faceted Pt NPs as a function of temperature. Dashed lines indicate the initial values at low temperatures.

Apparently, different shapes have different initial values (see the dashed lines in Fig. 7). Because each NP can retain its original shape well at the low temperatures (typical below 800 K), it is natural to find that the shape factors of NPs basically kept constant in the low temperature region. Slight fluctuations around the original value should be attributed to the thermally driven motions of atoms at non-zero temperatures. When the temperature was further increased, all the shape factors began to distinctly deviate from the dashed lines to different extents, indicating the rapid diffusion of surface atoms and the initialization of shape transformation. The critical temperature at which the shape factor begins to continuously decrease or increase is ascertained to be 1450, 1350, 1250 K for the TPHs covered by {211}, {311}, {411} facets, 1000, 1000, 1000 K for the TOHs by {221}, {331}, {441} ones, and 1300, 1200, 1200 K for the THHs by {210}, {310}, {410} ones, respectively. It should be noted that the critical temperature is much lower than the corresponding melting point, signifying the shape transformation of NP prior to its melting. However, the shape stability seems to be not consequentially associated with the thermal stability or surface energy. For examples, the {221} faceted TOH NP, which possesses the highest melting point among these high-index-faceted NPs, is found to have the lowest critical temperature for shape transformation; the {210}

faceted THH NP, which has the highest surface energy, can keep its shape at higher temperatures than the {310}, and {410} faceted ones and even TOH NPs. Besides, the shape of the {441} faceted TOH transformed more easily than that of the {411} faceted TPH although their melting points and surface energies are very close (see the discussion in Section 3.1 and 3.2). Despite the different polyhedral shapes, the shape factors of all the NPs converged to a constant of 0.44 or so at high temperatures, implying that all of them were evolved into the same spherical shapes after completely melting, consistent with the snapshots in Fig. 6.

Why do the high-index-faceted NPs exhibit diverse shape stabilities? To explore the origination of shape stability, we will take the TPH NPs as representatives to examine their shape evolutions. Fig. 8 demonstrates the shape changes of TPH Pt NPs with different high-index facets taken at four representative temperatures during heating process. In order to highlight the atomic diffusion behavior, we classified all atoms into two categories according to their CNs at the initial configurations. Atoms with twelve-fold coordination were regarded as interior atoms, otherwise surface atoms.

In accord with Fig. 7, the {211} and {311} faceted TPH NPs can maintain their original surface structures well at the temperature up to 800 K or so (see Fig. 8a and 8b), while the corresponding temperature for the {411} faceted one was about 700 K (see Fig. 8c). Generally, the less-coordinated atoms are easier to diffuse as the temperature is elevated. Therefore, the initial transformation of surface structure is mainly dependent on the CN distribution of those atoms located at apexes and kinks. The common neighbor analysis showed that the numbers of three- and four-coordinated atoms are zero and six for the {211} and {311} faceted TPHs while eight and zero for the {411} one. This partly explains why the former possess relatively better shape stability than the latter. At 1100 K, the corner atoms near kinks and the outer terraces have firstly moved away from their initial positions. With the temperature further rising, more and more less-coordinated atoms left, resulting in the exposure of the increasing interior atoms on the surface. At 1400 K, the facets and shape of the {211} faceted NP are still distinguishable although the corner atoms have already disappeared and the edges have been obtuse. However, the other two NPs have lost their initial facets. Note that the critical temperature of shape transformation is 1350 K and 1250 K for the {311} and {411} faceted NPs, respectively. By common neighbor analysis, it is found that the average coordination number of surface atoms is 8.471, 8.309, and 8.213 for the {211}, {311}, and {411} faceted TPH NPs, indicating that the high coordination number of surface atoms is beneficial to enhancing the shape stability. The available study has confirmed that those atoms on {111} facets have nine-fold coordination and can keep their fcc arrangements at a relatively high temperature of 1700 K or so[58]. Hence, it is expectable that a large proportion of high-coordinated surface atoms whose CNs are not less than nine would be in favor of the shape stability of TPH. The calculated results showed that the proportion of these atoms on the surface is 0.6279, 0.4831, 0.3854 for the {211}, {311}, {411} faceted NPs, respectively. This also corroborates the fact that the shape stability comply with the order of {211} > {311} > {411} faceted TPH. When the temperature was further increased, the diffusion of both surface and interior atoms became progressively intense. At 1700 K, the orderly surface structures have been completely destroyed and the TPH shape became not differentiable. Subsequently, the NPs would initiate to the surface melting and finally evolve into sphere ones.

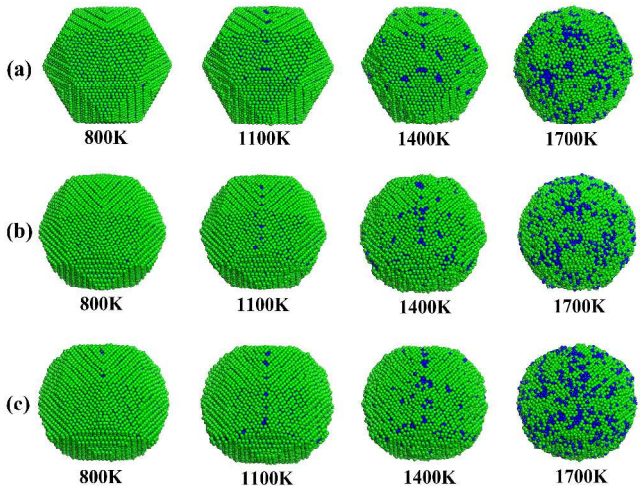

Fig. 8 Snapshots of Trapezohedral Pt NPs with different Miller index facets taken at four representative temperatures. (a) {211}, (b) {311}, and (c) {411} facets. Coloring denotes type of atom: green, surface atom; blue, interior atom.

As for the TOHs, the average coordination number of surface atoms is very close (8.804, 8.799, and 8.806 for the {221}, {331}, and {441} faceted NPs, respectively). Moreover, the proportion of high-coordinated surface atoms whose CNs are not less than nine is 0.651, 0.6496, and 0.6101 for the {221}, {331}, and {441} faceted ones, respectively. Therefore, these three TOH NPs presented the similar diffusion behavior and the similar critical temperature of shape transformation. As for the THHs, the {210} faceted NP exhibited better shape stability than the {310} and {410} ones although the surface energy of the former is higher than those of the latter. By analysis of the coordination number, it is found that the average coordination number of surface atoms is 8.473, 8.363, 8.212 for the THH NPs bound by {210}, {310}, {410} facets, respectively. Moreover, the proportion of high-coordinated surface atoms whose CNs are not less than nine is 0.6154, 0.4452, 0.34 for the {210}, {310}, {410} faceted THH NPs, respectively. Therefore, the shape stability of THH decreases according to the order of {210}, {310} and {410} faceted NPs. The aforementioned results imply that for the same polyhedron (TPH, TOH, or THH), the shape stability is strongly dependent on the CNs of surface atoms and their distributions.. By the comparison of different polyhedra, the particle shape closer to the sphere has better shape stability. For example, the TPH is closest to the sphere among three types of polyhedra (see the illustration in Fig. 1 and the shape factor in Fig. 7), therefore it holds the best shape stability. Contrarily, the shape factor of TOH is the farthest from that of sphere among all these polyhedra and its shape stability is the worst. Naturally, the THH lies between the TPH and TOH in shape stability.

4. Conclusions

In summary, atomistic simulations have been employed to systematically investigate the structure and stability of high-index-

faceted Pt NPs. The Lindemann index, shape factor, and coordination number were adopted to explore the melting mechanism and shape evolution of these NPs during continuous heating process. The major conclusions are summarized as follows:

1. The structural stability of polyhedral NPs roughly rises in the order of THH<TPH<TOH. {211} faceted TPH NPs exhibit the best stability when the NP sizes are between 4.5 nm and 25.9 nm, otherwise {221} faceted TOH NPs are the most stable. In contrast, {410} faceted THH NPs display worst structural stability.

2. {221} faceted TOH and {211} faceted TPH NPs possess the best and second-best thermal stability, respectively, while {410} faceted THH NPs do the worst.

3. Generally, the shape stability for three types of polyhedral NPs comply with the order of TOH<THH<TPH.

4. For the same type of polyhedron, the structural, thermal and shape stabilities of NPs covered by different high-index-facets all decrease according to the order of {2*kl*}, {3*kl*} and {4*kl*}.

These results revealed that the structural stability of NPs is determined not only by their surface energy but also by other factors such as the ratio of surface atoms to total number of atoms. Although the low surface energy is beneficial to the structural and thermal stabilities of these NPs, it is also accompanied with the low dangling bond density of surface and the decreasing catalytic activity. Additionally, a large proportion of high-coordinated surface atoms (CN$\geqslant$9) are helpful for enhancing both the thermal and the shape stabilities since the low-coordinated sites generally initiate the atomic diffusion and surface premelting. However, the shape stability is not necessarily associated with the thermal or structural stability. For different polyhedra, the particle shape closer to the sphere has better shape stability. For the same type of polyhedron, the shape stability is mainly determined by the average coordination number of surface atoms and their distributions. All these results demonstrate that the stability and catalytic property of Pt NPs could be tunable by altering their shapes and surface structures. This study is of considerable importance not only for in-depth understanding of surface structures and thermodynamic properties of high-index-faceted NPs but also for the design and synthesis of high-index-faceted noble metal NPs with both high catalytic activity and excellent stability.

Acknowledgements

This work is supported by the National Natural Science Foundation of China (Grant Nos. 51271156 and 11204252), the Natural Science Foundation of Fujian Province of China (Grant No. 2013J06002), and the Specialized Research Fund for the Doctoral Program of Higher Education of China (Grant No. 20130121110012).

Notes and references

* E-mail: yhwen@xmu.edu.cn (Y. H. Wen).
Phone: (+86) 592-218-2248. Fax: (+86) 592-218-9426.

[a] Institute of Theoretical Physics and Astrophysics, Department of Physics, Xiamen University, Xiamen 361005, China
[b] Research Center for Cloud Computing and Big Data, Department of Automation, Xiamen University, Xiamen, 361005, China
[c] State Key Laboratory of Physical Chemistry of Solid Surfaces, Department of Chemistry, Xiamen University, Xiamen 361005, China

1 A. T. Bell, *Science*, 2003, **299**, 1688–1691.
2 R. Ferrando, J. Jellinek and R. L. Johnston, *Chem. Rev*., 2008, **108**, 846–910.
3 Z. Y. Zhou, N. Tian, J. T. Li, I. Broadwell and S. G. Sun, *Chem. Soc. Rev*., 2011, **40**, 4167–4185.
4 Z. L. Wang, *J. Phys. Chem. B*, 2000, **104**, 1153–1175.
5 R. Narayanan and M. A. El–Sayed, *Nano Lett.*, 2004, **4**, 1343–1348.
6 H. Lee, S. E. Habas, S. Kweskin, D. Butcher, G. A. Somorjai and P. D. Yang, *Angew. Chem. Int. Ed.*, 2006, **45**, 7824–7828.
7 K. M. Bratlie, H. Lee, K. Komvopoulos, P. Yang and G. A. Somorjai, *Nano Lett.*, 2007, **7**, 3097–3101.
8 C. K. Tsung, J. N. Kuhn, W. Y. Huang, C. Aliaga, L. I. Hung, G. A. Somorjai and P. D. Yang, *J. Am. Chem. Soc.*, 2009, **131**, 5816–5822.
9 T. S. Ahmadi, Z. L. Wang, T. C. Green, A. Henglein and M. A. El–Sayed, *Science*, 1996, **272**, 1924–1926.
10 Y. G. Sun and Y. N. Xia, *Science*, 2002, **298**, 2176–2179.
11 X. Fu, Y. Wang, N. Wu, L. Gui and Y. Tang, *Langmuir*, 2002, **18**, 4619–4624.
12 H. Song, F. Kim, S. Connor, G. A. Somorjai and P. Yang, *J. Phys. Chem. B*, 2005, **109**, 188–193.
13 J. T. Ren and R. D. Tilley, *J. Am. Chem. Soc.*, 2007, **129**, 3287–3291.
14 J. Y. Chen, B. Lim, E. P. Lee and Y. N. Xia, *Nano Today*, 2009, **4**, 81–95.
15 S. L. Bernasek and G.A. Somorjai, *Surf. Sci.*, 1975, **48**, 204–213.
16 N. P. Lebedeva, M. T. M. Koper, J. M. Feliu and R. A. van Santen, *J. Phys. Chem. B*, 2002, **106**, 12938–12947.
17 N. Tian, Z. Y. Zhou and S. G. Sun, *J. Phys. Chem. C*, 2008, **112**, 19801–19817.
18 N. Tian, Z. Y. Zhou, S. G. Sun, Y. Ding and Z. L. Wang, *Science*, 2007, **316**, 732–735.
19 Z. Y. Zhou, Z. Z. Huang, D. J. Chen, Q. Wang, N. Tian and S. G. Sun, *Angew. Chem. Int. Ed.*, 2010, **49**, 411–414.
20 T. Ming, W. Feng, Q. Tang, F. Wang, L. D. Sun, J. F. Wang and C. H. Yan, *J. Am. Chem. Soc.*, 2009, **131**, 16350–16351.
21 J. Li, L. H. Wang, L. Liu, L.Guo, X. D. Han and Z. Zhang, *Chem. Commun.*, 2010, **46**, 5109–5111.
22 N. Tian, Z. Y. Zhou, N. F. Yu, L. Y. Wang and S. G. Sun, *J. Am. Chem. Soc.*, 2010, **132**, 7580–7581.
23 C. L. Lu, K. S. Prasad, H. L. Wu, J. A. A. Ho and M. H. Huang, *J. Am. Chem. Soc.*, 2010, **132**, 14546–14553.
24 Y. J. Deng, N. Tian, Z. Y. Zhou, R. Huang, Z. L. Liu, J. Xiao and S. G. Sun, *Chem. Sci.*, 2012, **3**, 1157–1161.
25 Z. Y. Zhou, N. Tian, Z. Z. Huang, D. J. Chen and S. G. Sun, *Faraday Discuss.*, 2008, **140**, 81–92.
26 Y. Y. Li, Y. X. Jiang, M. H. Chen, H. G. Liao, R. Huang, Z. Y. Zhou, N. Tian, S. P. Chen and S. G. Sun, *Chem. Commun.*, 2012, **48**, 9531–9533.
27 Y. Y. Ma, Q. Kuang, Z. Y. Jiang, Z. X. Xie, R. B. Huang, L. S. Zheng, *Angew. Chem. Int. Ed.*, 2008, **47**, 8901–8904.
28 M. Eguchi, D. Mitsui, H. L. Wu, R. Sato and T. Teranishi, *Langmuir*, 2010, **26**, 12307–12313.
29 L. Zhang, W. X. Niu, Z. Y. Li and G. B. Xu, *Chem. Commun.*, 2011, **47**, 10353–10355.
30 J. Xiao, S. Liu, N. Tian, Z. Y. Zhou, H. X. Liu, B. B. Xu and S. G. Sun, *J. Am. Chem. Soc.*, 2013, **135**, 18754–18757.
31 Y. N. Wen and J. M. Zhang, *Solid State Commun.*, 2007, **144**, 163–167.
32 J. M. Sun, D. Ma, H. Zhang, X. M. Liu, X. W. Han, X. H. Bao, G. Weinberg, N. Pfaender and D. S. Su, *J. Am. Chem. Soc.*, 2006, **128**, 15756–15764.
33 T. Cagin, Y. Kimura, Y. Qi, H. Li, H. Ikeda, W. L. Johnson and W. A. Goddard, *Mater. Res. Soc. Symp. Proc.*, 1999, **554**, 43–48.
34 M. S. Daw and M. I. Baskes, *Phys. Rev. Lett.*, 1983, **50**, 1285–1288.
35 M. S. Daw and M. I. Baskes, *Phys. Rev. B*, 1984, **29**, 6443–6453.
36 H. Ikeda, Y. Qi, T. Cagin, K. Samwer, W. L. Johnson and W. A.

Goddard, *Phys. Rev. Lett.*, 1999, **82**, 2900–2903.
37 Y. Qi, T. Cagin, W. L. Johnson and W. A. Goddard, *J. Chem. Phys.*, 2001, **115**, 385–394.
38 S. K. R. S. Sankaranarayanan, V. R. Bhethanabotla and B. Joseph, *Phys. Rev. B*, 2005, **72**, 195405.
39 Y. H. Wen, Y. Zhang, J. C. Zheng, Z. Z. Zhu and S. G. Sun, *J. Phys. Chem. C*, 2009, **113**, 20611–20617.
40 R. Huang, Y. H. Wen, Z. Z. Zhu and S. G. Sun, *J. Mater. Chem.*, 2011, **21**, 11578–11584.
41 R. Huang, Y. H. Wen, Z. Z. Zhu and S. G. Sun, *J. Phys. Chem. C*, 2012, **116**, 8664–8671.
42 Y. H. Wen, R. Huang, C. Li, Z. Z. Zhu and S. G. Sun, *J. Mater. Chem.*, 2012, **22**, 7380–7386.
43 A. R. Leach, Molecular Modelling: Principles and Applications, Prentice–Hall, London, 2001.
44 D. J. Evans and B. L. Holian, *J. Chem. Phys.*, 1985, **83**, 4069–4074.
45 H. J. C. Berendsen, J. P. M. Postma, W. F. van Gunsteren, A. DiNola and J. R. Haak, *J. Chem. Phys.*, 1984, **81**, 3684–3690.
46 W. C. Swope, H. C. Andersen, P. H. Berens and K. R. Wilson, *J. Chem. Phys.*, 1982, **76**, 637–649.
47 G. A. Breaux, C. M. Neal, B. Cao and M. F. Jarrold, *Phys. Rev. Lett.*, 2005, **94**, 173401.
48 J. Kang, S. H. Wei and Y. H. Kim, *J. Am. Chem. Soc.*, 2010, **132**, 18287–18291.
49 C. Kittel, Introduction to Solid State Physics, John Wiley & Sons: New York, 1996.
50 Y. H. Wen, H. Fang, Z. Z. Zhu and S. G. Sun, *Chem. Phys. Lett.*, 2009, **471**, 295–299.
51 Q. S. Mei and K. Lu, *Prog. Mater. Sci.*, 2007, **52**, 1175–1262.
52 Y. H. Wen, R. Huang, X, M. Zeng, G. F. Shao and S. G. Sun, *J. Mater. Chem. A*, 2014, **2**, 1375–1382.
53 H. Lowen, *Phys. Rep.*, 1994, **237**, 249–324.
54 Y. Shibuta and T. Suzuki, *Chem. Phys. Lett.*, 2007, **445**, 265–270.
55 Y. Q. Zhou, M. Karplus, K. D. Ball and R. S. Berry, *J. Chem. Phys.*, 2002, **116**, 2323–2329.
56 B. Cao, A. K. Starace, O. H. Judd and M. F. Jarrold, *J. Am. Chem. Soc.*, 2009, **131**, 2446–2447.
57 Z. L. Wang, Z. Q. Zhong and S. Y. Wang, *Text. Res. J.*, 2012, **82**, 454–462.
58 Y. H. Wen, H. Fang, Z. Z. Zhu and S. G. Sun, *Phys. Lett. A*, 2009, **373**, 272–276.

BRIEFS

Atomistic simulations are used to investigate the structural, thermal and shape stabilities of Pt nanoparticles with high-index facets.

GRAPHICAL ABSTRACT